The evolution of tides and tidal dissipation over the past 21,000 years

Wilmes, S.B.; Green, J.A.M.

Journal of Geophysical Research: Oceans

DOI:
10.1002/2013JC009605

Published: 07/07/2014

Publisher's PDF, also known as Version of record

AGU PUBLICATIONS

JGR

Journal of Geophysical Research: Oceans

RESEARCH ARTICLE
10.1002/2013JC009605

The evolution of tides and tidal dissipation over the past 21,000 years

S.-B. Wilmes[1] and J. A. M. Green[1]

[1]School of Ocean Sciences, College of Natural Sciences, Bangor University, Menai Bridge, UK

Key Points:
- M2 tidal amplitudes and dissipation were strongly enhanced during the LGM
- Changes in the LGM K1 tides were confined to areas where K1 dominates today
- The deglacial M2 tides were closely linked to ice sheet groundling line locations

Correspondence to:
S.-B. Wilmes,
s.wilmes@bangor.ac.uk

Citation:
Wilmes, S.-B., and J. A. M. Green (2014), The evolution of tides and tidal dissipation over the past 21,000 years, *J. Geophys. Res. Oceans*, *119*, 4083–4100, doi:10.1002/2013JC009605.

Received 11 NOV 2013
Accepted 13 JUN 2014
Accepted article online 16 JUN 2014
Published online 7 JUL 2014

Abstract The 120 m sea-level drop during the Last Glacial Maximum (LGM; 18–22 kyr BP) had a profound impact on the global tides and lead to an increased tidal dissipation rate, especially in the North Atlantic. Here, we present new simulations of the evolution of the global tides from the LGM to present for the dominating diurnal and semidiurnal constituents. The simulations are undertaken in time slices spanning 500–1000 years. Due to uncertainties in the location of the grounding line of the Antarctic ice sheets during the last glacial, simulations are carried out for two different grounding line scenarios. Our results replicate previously reported enhancements in dissipation and amplitudes of the semidiurnal tide during LGM and subsequent deglaciation, and they provide a detailed picture of the large global changes in M_2 tidal dynamics occurring over the deglaciation period. We show that Antarctic ice dynamics and the associated grounding line location have a large influence on global semidiurnal tides, whereas the diurnal tides mainly experience regional changes and are not impacted by grounding line shifts in Antarctica.

1. Introduction

The 120–130 m ice-equivalent sea-level reduction during the Last Glacial Maximum (LGM; some 22,000–18,000 years before present; henceforth 22–18 kyr BP) had a significant impact on the tides on a variety of scales due to the exposure of the continental shelf seas [e.g., *Egbert et al*., 2004; *Arbic et al*., 2004; *Uehara et al*., 2006; *Griffiths and Peltier*, 2008, 2009; *Green*, 2010; *Hill et al*., 2011; *Hall et al*., 2013]. The main effect on the tides was the increase of the total amount of semidiurnal tidal energy lost in the ocean during the LGM to levels far above present. Furthermore, the main part of this energy dissipated in the deep ocean and not in shallow shelf seas as is the case today [*Egbert and Ray*, 2001]. As the sea-level rose at the end of the glacial period the present-day shelf seas flooded and there was a subsequent shift in the tidal dissipation from the open ocean to the newly flooded shelf seas [e.g., *Egbert et al*., 2004; *Uehara et al*., 2006; *Green*, 2010]. Here we present new simulations of the evolution of the near-global tides from the LGM to the present. The purpose of this investigation is threefold: (i) to present the evolution of the global semidiurnal tides at higher temporal and spatial resolutions than previously reported [e.g., *Egbert et al*., 2004; *Uehara et al*., 2006; *Hill et al*., 2011; *Hall et al*., 2013], (ii) to describe the evolution of the diurnal tides from the LGM to the present, and (iii) to investigate the sensitivity of the global tides at present and during the LGM to the location of ice sheet grounding lines, thus extending the work by *Griffiths and Peltier* [2009].

Previous simulations of the paleoocean tides show surprising results, with total globally integrated dissipation some 30% larger than at present and a larger fraction of this energy dissipating in the deep ocean [*Egbert et al*., 2004; *Green*, 2010]. The dissipation in the semidiurnal band increased far more than that of the diurnal constituents [*Green*, 2010], which implies that the mechanism behind these shifts is tidal resonance [*Egbert et al*., 2004; *Griffiths and Peltier*, 2008; *Arbic et al*., 2009; *Green*, 2010]. Removing the shelf seas effectively reduces the damping of the tides, which—when the ocean basin is close to resonance—leads to an increased tidal amplitude and associated dissipation of energy [see *Egbert et al*., 2004; *Green*, 2010, especially their Figures 11 and 1, respectively]. The present-day North Atlantic has natural resonant periods of 12.66, 12.8, and 14.4 h [*Platzman*, 1975; *Platzman et al*., 1981; *Müller*, 2008], which explains why there may have been megatides present there during the LGM [e.g., *Uehara et al*., 2006; *Arbic et al*., 2007; *Griffiths and Peltier*, 2008, 2009]. Furthermore, *Arbic et al*. [2009] and *Skiba et al*. [2013] show that adding a shelf ocean which is close to resonance to a deep ocean basin that is also close to resonance reduces the deep ocean tides of the ocean basin; this is analogous to when the European and Patagonian shelves flooded during the deglaciation after the LGM.

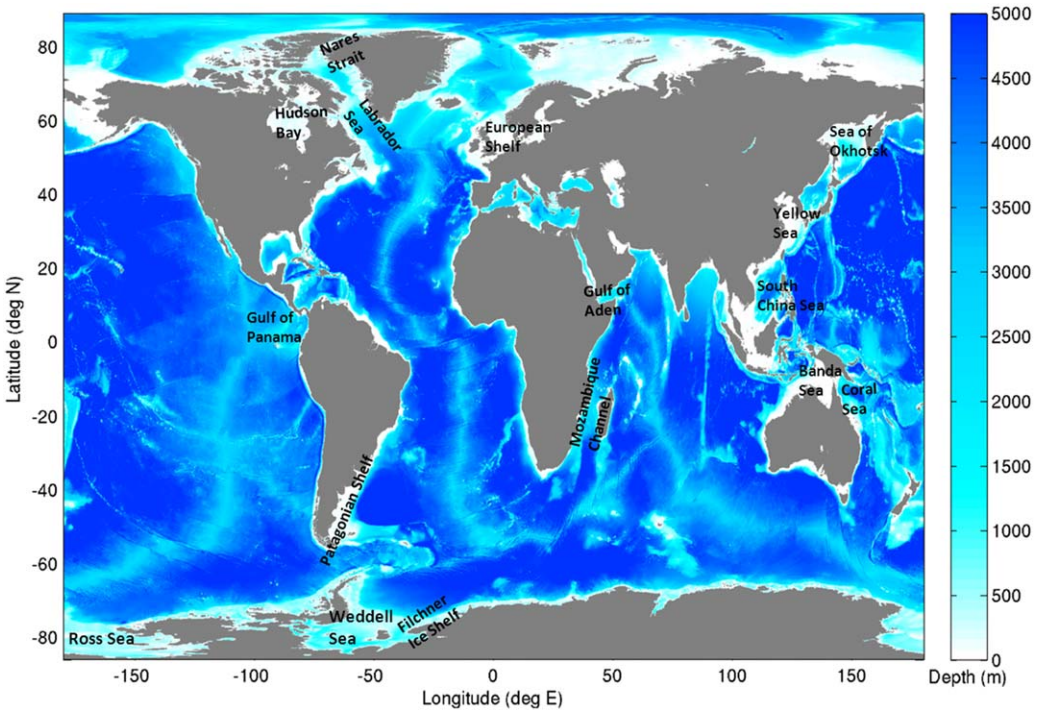

Figure 1. Present-day bathymetry assembled from the Smith and Sandwell, v.14, IBCAO, v.2, and ETOPO1 databases. Regions mentioned in subsequent sections of this paper are marked on the map.

The bathymetry under and the extent of floating ice shelves in Antarctica are important in determining the regional tidal dynamics [*Griffiths and Peltier*, 2009; *Rosier et al*., 2014]. However, there is an ongoing debate about the exact grounding line location of the Antarctic Ice Sheet during the LGM and the subsequent deglacial period. This is especially true for the Weddell Sea sector (see Figure 1), where estimates range from an ice sheet grounded at the shelf margin [e.g., *Hall and Denton*, 2000; *Larter et al*., 2012; *Anderson et al*., 2002] to an only partially grounded ice sheet within the Weddell Sea, with strongly differing estimates over the timing of the initiation of deglaciation [e.g., *Stolldorf et al*., 2012; *Hein et al*., 2011; *Hillenbrand et al*., 2012]. For the Western Ross Sea, however, there is a general consensus that the ice sheet grounded at the present-day shelf break during the LGM [e.g., *Anderson et al*., 2002; *Domack et al*., 1999; *Hall and Denton*, 2000; *McKay et al*., 2008; *Livingstone et al*., 2012]. Although the behavior of the ice masses in the Western Ross Sea has been extensively researched, ambiguity of both LGM extent and deglacial behavior exists for the Eastern Ross Sea [e.g., *Shipp et al*., 1999; *Anderson et al*., 2002; *Mosola and Anderson*, 2006]. *Griffiths and Peltier* [2009] investigate regional changes in the polar LGM tides in global tidal simulations in response to different grounding line locations of both the Antarctic Ice Sheet and the ice sheet occupying the Queen Elizabeth Islands in the Canadian Arctic and show that grounding line shifts affect the tides in the vicinity of the respective ice sheets. In our simulations, we extend the approach by *Griffiths and Peltier* [2009] and analyze the response in global tides to different grounding line positions of the Antarctic Ice Sheet from the LGM to the early Holocene.

There are several reasons to reinvestigate the tidal evolution over the last 21 kyr with higher resolution and with the response of both semidiurnal and diurnal tides described. Changes in tidal dissipation can affect the large scale meridional overturning circulation (MOC), which has been shown to be sensitive to the input of mechanical energy in the deep ocean [e.g., *Huang*, 1999; *Johnson et al*., 2008; *Green et al*., 2009]. Based on first-order physical principles [e.g., *Stommel*, 1961], it is thus expected that the MOC during the LGM would be stronger. Instead, most investigations point toward the MOC being more sluggish during in the past due to an increased freshwater input to the North Atlantic, which hampered the formation of North Atlantic Deep Water [e.g., *Broecker and Denton*, 1990; *Lenderink and Haarsma*, 1994; *Rahmstorf*, 2002; *Green et al*., 2009]. However, the increased energy input from tides during the LGM may have facilitated the recovery of the MOC at the end of any freshwater pulse [*Green et al*., 2009; *Green and Bigg*, 2011]. The very large

tides reported in the Arctic and Labrador Sea during the LGM may also have been acting to destabilize the continental ice sheets [*Arbic et al*., 2004; *Rosier et al*., 2014], and tides themselves are quite sensitive to the location of ice sheet grounding lines [*Griffiths and Peltier*, 2008, 2009; *Rosier et al*., 2014]. The present simulations thus provide a new insight into the behavior of the tides over the last 21 kyr at high resolution, and may form a basis for mixing in further climate models simulations.

In order to provide better tidal estimates for the last 21 kyr, we rerun the model used by *Egbert et al*. [2004] but with a slightly modified setup. We include most of the Arctic, as opposed to cutting at 82°N. We also include analysis of the K_1 tide, and we investigate the sensitivity of the global tidal evolution to the location of the Antarctic grounding lines. Furthermore, we present results from time slices every 500–1000 years from the LGM to the present, thus exploring new features of the tides not reported previously. Previous global studies have either presented selected time slices with spatially high resolution [*Egbert et al*., 2004; *Green*, 2010], coarse resolution studies with higher temporal resolution [*Thomas and Sündermann*, 1999; *Uehara et al*., 2006] or have shown temporally and spatially highly resolved regional timeslices [*Uehara et al*., 2006; *Hill et al*., 2011; *Hall et al*., 2013]. To date only regional changes in tides in response to changes in the grounding line location and ice shelf extent of the Antarctic Ice Sheet have been examined [*Griffiths and Peltier*, 2009; *Rosier et al*., 2014], whereas this study is carried out with both a high temporal and spatial resolution and looks at the global impacts of changes in the grounding line in Antarctica. We begin by introducing the tidal model in the next section, including an overview of the different simulations. The results for both the M_2 and K_1 constituents from these simulations are presented in section 3 where we first explore the LGM state and then investigate the temporal evolution from the LGM to the present.

2. Tidal Modeling

2.1. Model Description

The Oregon State University Tidal Inversion Software (OTIS) has been used in several previous investigations to simulate global and regional tides in the past, present, and future oceans [e.g., *Egbert et al*., 2004; *Green*, 2010; *Pelling and Green*, 2013; *Green and Huber*, 2013]. It provides a numerical solution to the shallow water equations, but the nonlinear advection terms and the horizontal diffusion are neglected without loss of accuracy [*Egbert et al*., 2004]. The only forcing is the astronomic tide-generating force, and energy is dissipated through a quadratic bed-friction term and a linear tidal conversion scheme representing the energy losses to internal tides. We thus solve

$$\frac{\partial \mathbf{U}}{\partial t} + f \times \mathbf{U} = -gh\nabla(\eta - \eta_{SAL}) + \mathbf{F}_b + \mathbf{F}_w + \mathbf{\Theta} \tag{1}$$

$$\frac{\partial \eta}{\partial t} = -\nabla \cdot \mathbf{U} \tag{2}$$

where $\mathbf{U} = \mathbf{u}h$ is the depth-integrated volume transport given by the velocity $\mathbf{u}$ times the water depth h, $\mathbf{f}$ is the Coriolis vector, η and η_{SAL} the tidal elevation and the self-attraction and loading elevation, respectively, $\mathbf{F}$ is the dissipative stress from bed friction (subscript b) and tidal conversion (subscript w), respectively, and $\mathbf{\Theta}$ is the astronomic tide-generating force. Self-attraction and loading (SAL) was implemented through the iterative scheme suggested by *Egbert et al*. [2004], and four iterations are performed for each simulation period.

The bed-friction is parameterized using a standard quadratic law: $\mathbf{F}_b = C_d \mathbf{U}|\mathbf{u}|/h$, where $C_d = 3 \times 10^{-3}$ is a drag coefficient, and $\mathbf{u}$ is the total velocity vector for all the tidal constituents. The tidal conversion term, F_w, is a vector given by

$$\mathbf{F}_w = C|\nabla h|^2 \frac{N_h \bar{N}}{8\pi^2 \omega}\mathbf{U} \tag{3}$$

where $C = 50$ is a scaling factor, ∇h the horizontal gradient of the topography, N the buoyancy frequency, N_h is the value of N at the seabed, $\bar{N}$ the average of N over depth of the entire water column, and ω the tidal

frequency. This is a slightly modified version of that given by *Zaron and Egbert* [2006] as described by *Green and Nycander* [2013]. It assumes a horizontally uniform abyssal stratification which is parameterized by the buoyancy frequency N through $N(z)=N_0\exp\left(\frac{-z}{1{,}300}\right)$ with $N_0 = 5.24 \times 10^{-3}$. We acknowledge that changes in stratification could be important for the LGM, but they have been studied elsewhere [e.g., *Egbert et al*., 2004; *Griffiths and Peltier*, 2009] and our focus is on evaluating changes in tides due to shifts in the grounding line position. The establishment of a more accurate stratification is work in progress and not part of the scope of this paper. N^2 may have been a factor 2 higher during the LGM [*Green et al*., 2009]. In any case, our present results are conservative since we use a reduced vertical stratification for the LGM. In order to test for sensitivity of the results to changes in stratification we perform simulations of the LGM tides with IT drag multiplied by factors 0.5 and 2 in order to evaluate the sensitivity of dissipation to offsets in stratification.

The PD bathymetric data, used as the basis for all simulations, are a conglomerate of the Smith and Sandwell database, v.14, [see *Smith and Sandwell*, 1997, and topex.ucsd.edu/pub/global_topo_1min for the latest version] (SS) and Arctic and Antarctic bathymetries from IBCAO, v.2, [see *Jakobsson et al*., 2008, and http://www.ngdc.noaa.gov/mgg/bathymetry/arctic/downloads.html] and ETOPO1 databases [see *Amante and Eakins*, 2009, and http://www.ngdc.noaa.gov/mgg/global/], respectively (Figure 1). All data sets were averaged to 1/8° × 1/8° horizontal resolution and then linearly interpolated to a common latitude-longitude grid. In the southern part of the domain, ETOPO1 and SS are merged from 65° to 60° S using linear weighting. The same methodology is applied in the subpolar north where SS and IBCAO are merged between 74° and 79° N.

The paleotopography comes from ICE-5G [see *Peltier*, 2004, and http://www.atmosp. physics.utoronto.ca/peltier/data.php for the latest version], which has a 1° × 1° resolution and is available in 500 or 1000 year time slices from the present to the LGM. For accuracy reasons, the runs were also made on a 1/8° × 1/8° grid, with paleobathymetries obtained following the methodology in *Egbert et al*. [2004]: for each time slice, the difference between the 1° × 1° paleobathymetry and the 1° × 1° version of the present-day (PD) bathymetry was computed and then linearly interpolated to the PD 1/8° grid and added to the present-day 1/8° bathymetry. This leads to sea-level adjustment consistent with the ICE-5G database, but with the necessary resolution to obtain reliable results. The model grid thus has a fully global longitudinal span and covers the globe between 86°S and 89°N in latitude. At the northernmost boundary, an elevation boundary condition was applied using data from the TPXO7.2 database [see *Egbert and Erofeeva*, 2002, and http://volkov.oce.orst.edu/tides/global.html]. Simulations with a landmass at the northernmost boundary were done for a few select time slices and did not change the results [e.g., *Egbert et al*., 2004; *Arbic et al*., 2009], and we opted for the open boundary in the Arctic here. However, the fully global simulations in *Griffiths and Peltier* [2008, 2009] suggest that the tide was almost an order of magnitude larger along 89°N during the LGM—a feature which must have been crucial to generate their "megatides" along the Arctic shelf. As described later, we therefore performed sensitivity simulations with enhanced tidal amplitudes in our boundary conditions.

The present day runs were evaluated against the TPXO8 database which was averaged from a 1/30° × 1/30° to 1/8° × 1/8° horizontal resolution and then interpolated using linear interpolation to the common latitude-longitude grid. Note that for computational reasons, we still use TPXO7.2 for the boundary conditions—the difference between the two databases is negligible along 89°N and should not impact on the results—but, TPXO8 is generally more accurate due to the increased resolution.

2.2. Grounding Line Scenarios

LGM to early Holocene (21–10 kyr BP) simulations were carried out for two extreme grounding line cases in order to take the uncertainties of the reconstructions discussed in section 1 into account and to provide a realistic range in which "partially" grounded cases could lie. The first case deals with grounded Antarctic ice shelves (ice in Weddell and Ross Sea grounded, henceforth referred to as "GR"), whereas the second case uses floating Antarctic ice shelves (ice in Weddell and Ross Sea floating, "FL"). For the GR case all Antarctic ice given by the ice thickness data in the ICE-5G data set is assumed to be grounded. For the FL case the change in ice thickness between the paleo-slices and the present-day case is added to the total water depth and only when the ice thickness exceeds the height of the water column is the ice grounded; otherwise we assume that a floating ice shelf is present. The horizontal extent of the floating ice shelf is the same as for

the grounded ice sheet. We do not specify the thickness of the ice shelves as it is the total water depth change, i.e., the eustatic and isostatic sea level changes together with alterations water depth due to the displacement of water from the presence of ice shelves, and the location of the grounding line that are important for the tidal dynamics [e.g., *Griffiths and Peltier*, 2009; *Rosier et al*., 2014]. Throughout the Holocene we assumed the ice to have been ungrounded in the Weddell and Ross Sea and only the FL case is referred to for this period.

2.3. Simulations and Computations

Runs were made for the present and for a number of paleo time slices between 21 kyr BP and 1 kyr BP using the relevant topography for each time slice (the simulated ages are marked in Figure 7). The simulation period for each run was 13 days, of which the last 5 days were used for harmonic analysis of the modeled elevations and currents. Forcing consisted of the astronomic tidal potential and prescribed elevations at the Arctic boundary for the M_2 and K_1 constituents. Runs were made for the LGM (21 kyr) and the present using M_2, S_2, K_1, and O_1 forcing, using a 45 day run time with 30 day harmonic analysis, but the S_2 signal responds very similarly to M_2, and O_1 is close to K_1 in response, so for computational economy we focus on M_2 and K_1 in the following. Model output consists of tidal amplitudes and phases, and volume transports and transport phases for each modeled constituent. In order to test for the sensitivity to variations in the elevation boundary conditions at the northern open boundary (89°N) we performed runs where the TPXO7.2 boundary conditions were multiplied by factors of 2, 4, and 8 for the 21 kyr time slice with grounded Antarctic ice sheets.

The dissipation of tidal energy was computed following the methodology in *Egbert and Ray* [2001]. By taking $\mathbf{u}\cdot(1)+\eta g$ (2) and introducing the energy density $\rho_0 0.5[h\mathbf{u}^2+g\eta^2]$ which is assumed to be in steady state, the well-known expression for tidal dissipation D (in W m^{-2}) can be derived (after taking a time-average):

$$D=W-\nabla\cdot\mathbf{P} \tag{4}$$

Here, the work rate, W, and the divergence of the energy flux, $\mathbf{P}$, are defined as

$$W=g\rho_0\langle\mathbf{U}\cdot\nabla(\eta_{eq}+\eta_{SAL})\rangle \tag{5}$$

$$\mathbf{P}=g\rho_0\langle\mathbf{U}\eta\rangle \tag{6}$$

in which $\langle\rangle$ denote the time-averages. Using tidal amplitudes and currents from either the TPXO data base (for validation) or from the model simulations it is therefore possible to calculate the dissipation rate for each constituent without the need to use parameterizations.

3. Global Tidal Dynamics

3.1. The Control Runs

The amplitude and dissipation fields for the PD control runs for M_2 and K_1 for both floating and grounded Antarctic ice shelves can be seen in Figures 2 and 3. The different present-day scenarios are from now on referred to as pdM2fl (present day, M_2 constituent and floating ice shelves), pdM2gr (present day, M_2 constituent and grounded ice shelves) for M_2, and pdK1fl and pdK1gr for the K_1 results, respectively. Note that the grounded PD simulation is a sensitivity case brought on by some global topographic data bases not having any bathymetry under the Antarctic ice shelves. The corresponding root mean square (RMS) amplitude errors, total and deep dissipation, and correlation coefficients between modeled and observed amplitudes are listed in Table 1.

Using TPXO8 as observations we obtain a RMS difference of below 6.8 cm between the modeled M_2 tidal amplitudes for the floating ice shelf case (Figure 2) and observed M_2 elevations, whereas in water deeper than 500 m, the RMS difference is below 3.9 cm, which shows a marked improvement to the simulations by *Egbert et al*. [2004]. The correlation coefficient between pdM2fl and TPXO8 is $r = 0.95$, thus explaining 90% of the variance in TPXO8 which implies that we capture both the absolute tidal amplitudes and the

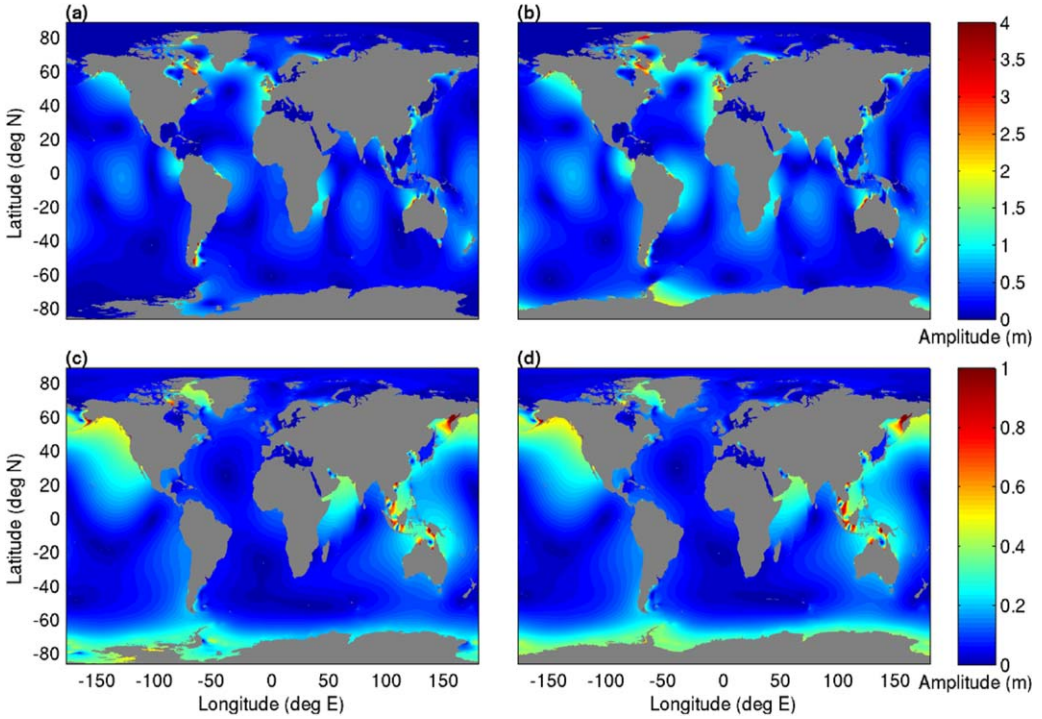

Figure 2. Present-day M_2 amplitudes for (a) floating and (b) grounded Antarctic ice shelves, respectively; (c) and (d) same but for K_1.

structure of the tidal elevation relatively well. For the grounded ice sheet case, pdM2gr, the RMS values are considerably higher with 16.6 and 12.8 cm for the whole ocean and the deep ocean, respectively. There is a marked offset in the tides around both Antarctica and in the North Atlantic region in this run, thus

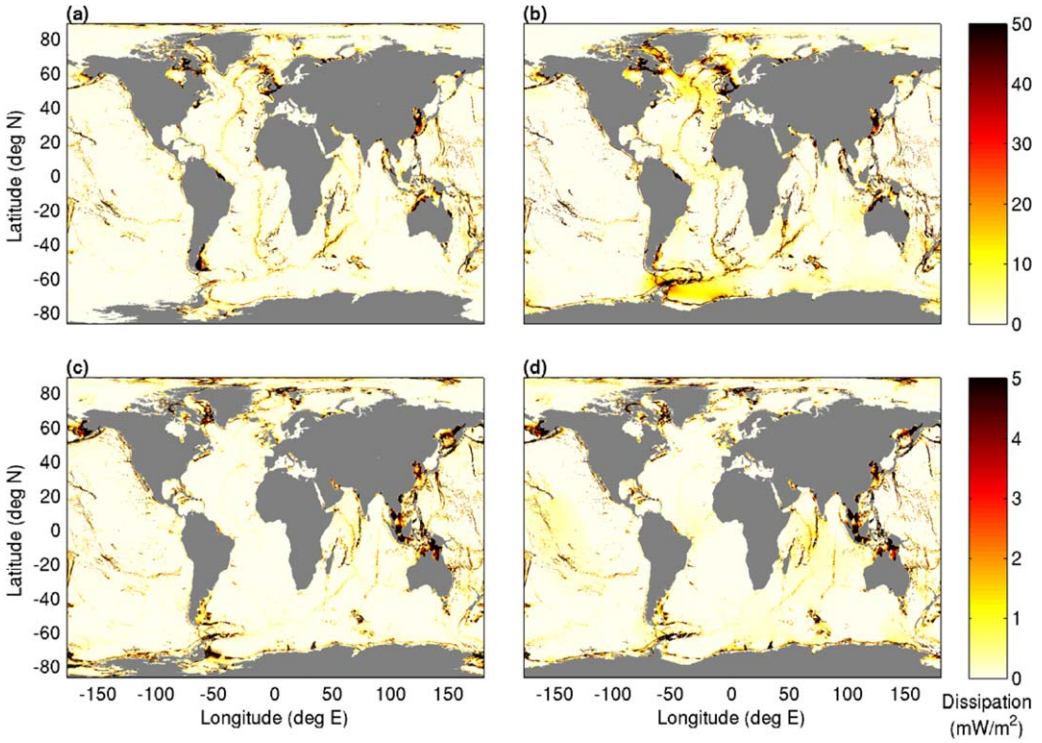

Figure 3. Same as Figure 2 but for dissipation.

Table 1. Comparison of Present-Day Simulations for Grounded and Floating Ice Shelves for M2 and K1, Respectively, to TPXO8[a]

Case	Total RMSE (cm)	Deep RMSE (cm)	Correlation Coefficient	Total Dissipation (TW)	Deep Dissipation (TW)
TPXO8 M2				2.393	0.957
TPXO8 K1				0.355	0.127
pdM2fl	6.671	3.866	0.947	2.291	0.957
pdM2gr	16.604	12.776	0.866	3.172	1.176
pdK1fl	2.838	1.771	0.926	0.380	0.174
pdK1gr	4.555	2.391	0.903	0.368	0.122

[a]Amplitude root mean square errors (RMSE) were calculated globally (first column; total RMSE) and for the deep ocean (depths > 500 m; second column; deep RMSE); the pattern correlations (third column; correlation coefficient) were obtained by correlating our elevation fields with the TPXO fields. The fourth and fifth columns show total and deep (>500 m) dissipation, respectively.

highlighting issues when using inaccurate Antarctic bathymetries and incorrect grounding line positions of the ice sheets. The grounding of the ice shelves around Antarctica leads to a marked increase in amplitude of several meters around Antarctica and a northward shift of the nearby amphidromic points, resulting in decreases in amplitudes along the south-east coast of South America and an increase along the central east coast (Figure 2). The shift in amphidromic points propagates all the way into the North Atlantic resulting in increased amplitudes in the Labrador Sea, the Nares Straits, and along the west coast of North America. In addition to the amplitude shifts by the blocking of the Weddell Sea, the grounded ice also acts as a wall which reflects tidal energy back into the North Atlantic, again resulting in a more energetic tidal field. These changes are also reflected in the dissipation field. Total M_2 dissipation for the FL case is 2.29 TW of which 0.96 TW (41%) takes place in the deep ocean (i.e., where $h > 500$ m). This compares very well with the deep dissipation from both TPXO8 (0.96 TW) and the estimates by *Egbert and Ray* [2001], but gives a very slight underestimate of the dissipation in shallow water, probably due to errors in the bathymetry. For the GR case, the dissipation increases considerably to 3.17 TW total and 1.18 TW (37%) deep dissipation, respectively. Here, a shift in dissipation occurring from the Patagonian shelf into Drake Passage and the Atlantic part of the Southern Ocean takes place, and the North Atlantic becomes significantly more energetic as seen from the amplitudes. This shows that a regional change in bathymetry can lead to significant alterations of global tidal dynamics.

The RMS error for pdK1fl is below 3 cm for the global tides and less than 1.8 cm for the deep ocean. The pattern correlation between TPXO8 and pdK1fl is $r = 0.93$ and our model result thus explains 86% of the variance in the TPXO8. For the grounded ice shelf case (pdK1gr), the RMS values are larger than for the floating case (pdK1fl), with values of 4.5 and 2.4 cm for the global and deep ocean, respectively. With grounded ice shelves the explained variance is reduced by 8%. For K_1, the difference between grounded and floating ice shelves is much less pronounced as for M_2 and the shifts in amplitude are local and confined to the proximity of Antarctica. For the GR case a pronounced decrease in dissipation can be seen in this region in comparison to the FL case, whereas only small changes occur throughout the remaining ocean. Total dissipation for the FL case is 0.38 TW with 45% of the dissipation taking place in the deep ocean giving a good fit with the TPXO8 data. For the grounded case total dissipation does not change but the fraction of deep dissipation decreases to 33%, as dissipation previously occurring in the Weddell and Ross Seas is omitted, and the Antarctic shelf and the Indian Ocean become more energetic.

3.2. Tidal Evolution

In this section, the evolution of the tides from 21 kyr BP to present is described for both M_2 and K_1 for each of the two grounding line scenarios. The LGM amplitude and dissipation fields can be seen in Figures 4 and 5. The evolution of dissipation globally is shown in Figure 7, and the corresponding basin wide dissipation is displayed in Figure 6.

3.2.1. M_2 Constituent

Global tidal dynamics at the LGM are strongly altered in comparison to the present-day case for both scenarios. For both grounding line cases, strongly enhanced tidal amplitudes and dissipation can be seen throughout the Atlantic, around Antarctica, the Coral Sea, the Gulf of Aden, the area north of the Mozambique Channel, and the Gulf of Panama (Figure 4). These areas correspond to areas of increased dissipation rates (Figure 5), and our results are consistent with those reported by *Egbert et al.* [2004] and *Griffiths and Peltier* [2008, 2009]. However, considerable differences can also be seen between the two different

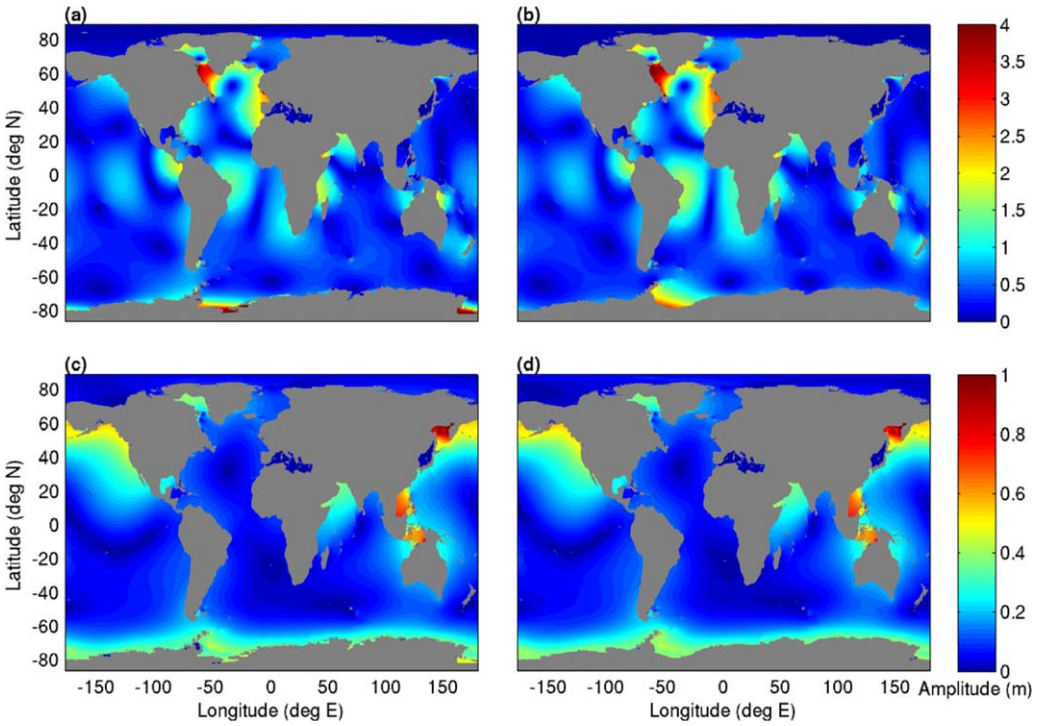

Figure 4. LGM (21 kyr BP) M_2 amplitudes for (a) floating and (b) for grounded Antarctic ice sheets, respectively. (c) and (d) same as Figures 4a and 4b but for K_1.

grounding line scenarios in both amplitudes and dissipation rates. At 21 kyr BP, the main differences in amplitude and dissipation between the grounding line scenarios are found in the Atlantic (Figure 6). In the South Atlantic and in the vicinity of Antarctica, the smallest amplitudes are observed for the grounded ice shelf case—the scenario which generates the largest tidal amplitudes in the North Atlantic region with a maximum of 5.5 m in the Labrador Sea. Ungrounding the ice sheet in both the Weddell and Ross Seas reduces the amplitude in the North Atlantic considerably, with the maximum amplitudes in the Labrador Sea dropping to 4.1 m. However, due to the formation of a shallow shelf sea in the Weddell Sea, considerable semidiurnal tidal amplitudes of up to 5.5 m can now also be seen here, and large tides can be observed in the Ross Sea. This corresponds to the results presented by *Griffiths and Peltier* [2009], who also find large changes in the regional Antarctic tides in response to grounding line shifts and report strongly enhanced tides in both the Ross and Weddell Sea for the LGM. They also find that the large tides in the Ross Sea disappear when the grounding line is advanced out toward the shelf break whereas the tides in the Weddell remain amplified with the grounding line shifts. These global differences in the tides due to grounding line changes are also reflected in the dissipation patterns which differ mainly in both the North and South Atlantic. Less energy is dissipated in the North Atlantic region as the Weddell Sea ice becomes ungrounded whereas for the South Atlantic the opposite is the case. The total M_2 dissipation estimates for the grounded case is 4.75 TW (GR), whereas the dissipation for the floating case is much lower at 4.05 TW (FL). The values mark an increase in dissipation compared to the FL present-day case by between 1.8 TW (78%) and 2.5 TW (107%) for the lowest and highest case, respectively. These values are in close correspondence to those previously reported [*Egbert et al*., 2004; *Uehara et al*., 2006; *Griffiths and Peltier*, 2008, 2009]. The reason for these differences in dissipation rates between the two scenarios becomes evident from Figures 5a and 5b. For the FL case the North Atlantic region tidal amplitudes are reduced in comparison to the GR scenario and less dissipation takes place south of Greenland. For the GR case, the grounding of the entire ice in the Weddell Sea and the removal of the shelf sea occupying the Weddell Sea enhances the Atlantic tides and increases dissipation in the North Atlantic. This is the same mechanism as discussed in *Egbert et al*. [2004] and *Green* [2010] where the removal of the damping factor (in this case the shelf sea in the Weddell Sea) in a basin that is in a near resonant state acts to enhance the dissipation in this system.

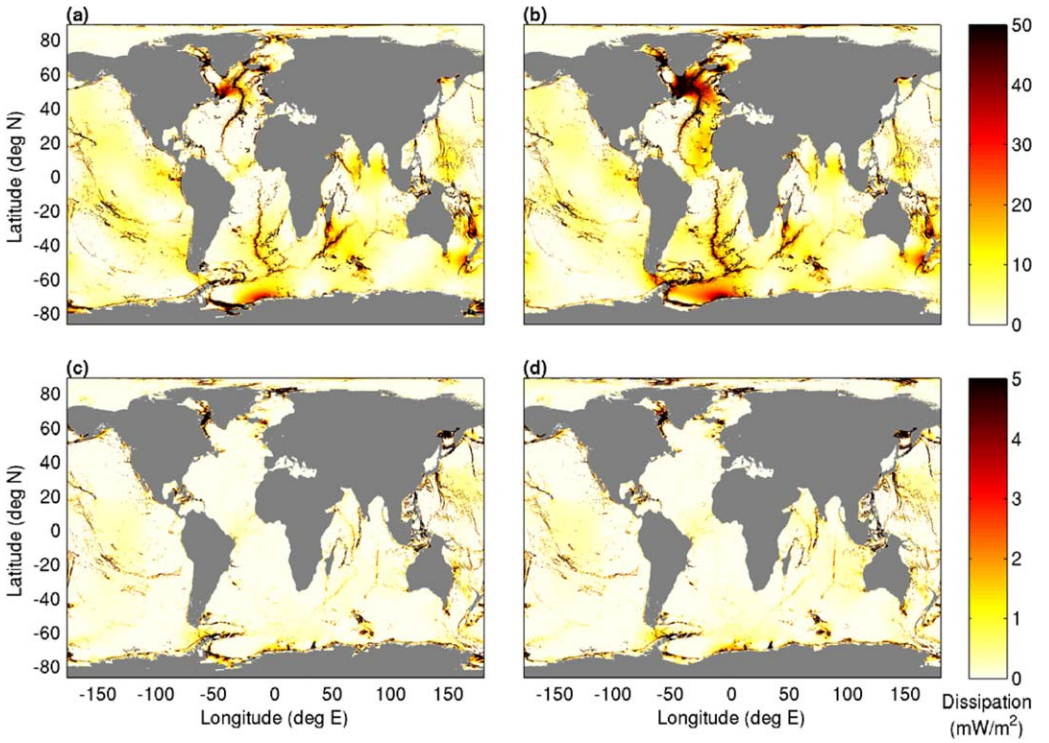

Figure 5. Same as Figure 4 but for dissipation.

We do not find the LGM "megatides" in the Arctic which *Griffiths and Peltier* [2008, 2009] see in their fully global simulations. Their results show M_2 amplitudes which exceed 3 m around the margins of the Artic basin, whereas we find tides in the Arctic basin which are strongly amplified by up to a factor of 5, but the absolute amplitudes are much smaller than those reported by *Griffiths and Peltier* [2008, 2009]. Increasing the elevation boundary conditions at the open boundary at 89°N by a factor of 2 leads to a small increase in the Arctic tides, whereas a factor 8 leads to an increase in amplitudes on the shelf close to those reported by *Griffiths and Peltier* [2009]. This also induces amplitudes along our boundary at 89°N which are consistent with those seen in *Griffiths and Peltier* [2009]. However, we find that altering the boundary conditions in the center of the Arctic has very little effect on the tides elsewhere on the globe outside the Arctic Basin, and changes are restricted to areas where the tides are large already and lie in the order of up to 5 cm. The same applies for dissipation rates, where the factor 8 boundary condition simulation produces an increase in global dissipation by 5% with the changes being local and restricted to the Arctic.

Large shifts in the global patterns of both amplitude and dissipation take place during the transition from the LGM to present that differ for each of the two grounding line scenarios for the semidiurnal tidal constituent. The changes during this period can be divided into four distinct phases over the time period under investigation:

3.2.1.1. 21–16 kyr BP

Between 21 and 18 kyr BP both amplitudes and dissipation rates largely reflect the LGM state and remain fairly constant throughout the period. Dissipation mainly occurs in waters deeper than 500 m, as most of the shelf seas were emergent during this period. Large tides can be observed in the Labrador Sea, along the European coast, and along the ice margins in the Weddell Sea. For both scenarios, the initial flooding of the shelf seas between 18 and 16 kyr BP leads to a slight drop in Labrador Sea amplitudes accompanied by an increase of the amplitudes on the European shelf. The dissipation rates remain constant over this period.

3.2.1.2. 16–10 kyr BP

As the shelf seas continue to flood pronounced drops in amplitudes and dissipation can be seen for both grounding line scenarios with dissipation shifting from the deep ocean to the shelf seas. The changes in

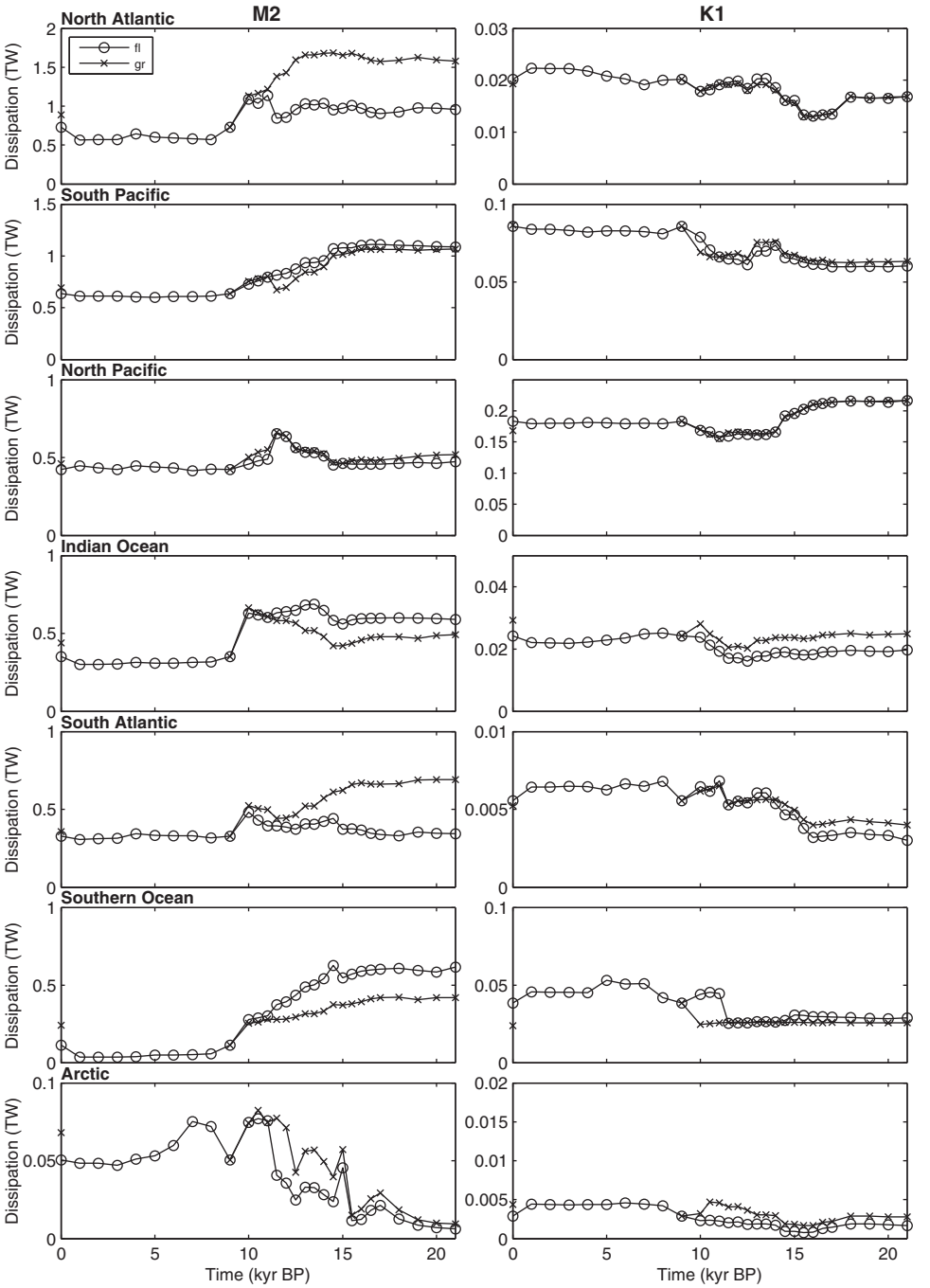

Figure 6. Regional total dissipation for M_2 and K_1 from 21 kyr BP to present for both GR and FL scenarios.

dissipation take place gradually and are more pronounced for the GR case with total dissipation decreasing by 0.8 TW, and deep dissipation by 1.8 TW. For the FL case, the drops amount to 0.4 and 1.3 TW, respectively (Figure 7). These figures correspond to the results presented by *Uehara et al.* [2006] who report decreases in dissipation of a very similar magnitude from simulations with a coarse resolution global tidal model for this time period. For the FL scenario, initially, the total dissipation remains fairly constant. A gradual decrease in amplitudes in the Labrador Sea can be seen commencing around 14 kyr BP corresponding to increased flooding of shelf seas which acts to reduce the deep dissipation rates. At this point, the dissipation in the Southern Ocean and South Atlantic also begin to drop whereas dissipation in the North Pacific and the

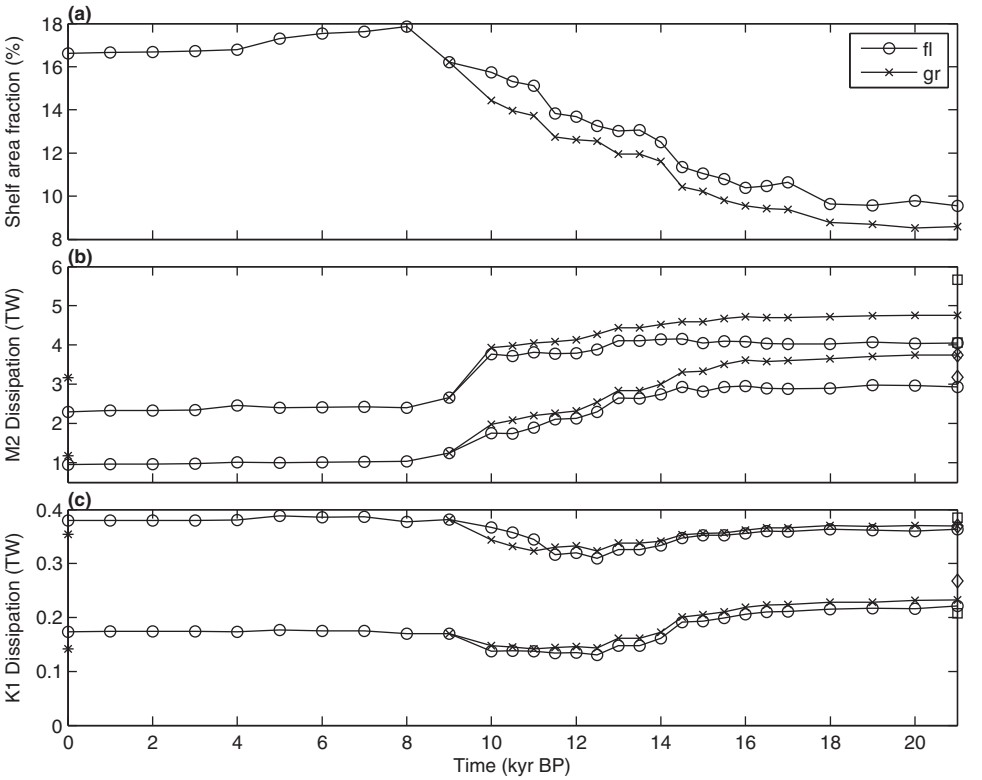

Figure 7. (a) Proportion of bathymetry that is shallower than 500 m; total (black) and deep (>500 m water depth, gray) dissipation for (b) M_2 and (c) K_1 for each of the for grounding line scenarios. Squares and diamonds mark the dissipation values for IT drag multiplied by a factor of 0.5 and 2, respectively. The stars at 0 kyr BP give the dissipation values for the grounded PD ice sheet case.

Indian Ocean increases due to the formation of new shallow seas. An especially pronounced drop in tidal amplitudes in the North Atlantic occurs between 12 and 11 kyr BP when the shelf area fraction increases by nearly 2% and parts of the Weddell and Ross Seas and the Patagonian Shelf flood. The flooding of these areas, which are all highly efficient dampers, consequently reduces the Atlantic tides and decreases dissipation. A large drop in dissipation can also be found in the North Pacific due to the flooding of the Yellow Sea. For the GR scenario both amplitudes and dissipation remain fairly constant in the North Atlantic region between 16 and 14 kyr BP, despite the large topographical changes. Decreases in dissipation can be seen in the Southern Ocean, South Atlantic and South Pacific. From 14 to 10 kyr BP pronounced changes in global tidal dynamics take place: tidal amplitudes in the Labrador Sea strongly decrease whereas large amplitudes can now be seen on the European Shelf. With the flooding of the shelf seas North Pacific and Indian Ocean dissipation initially increases, but for the Pacific the trend is reversed around 11.5 kyr when sea level rises abruptly.

3.2.1.3. 10–8 kyr BP

The most pronounced drop in global dissipation takes place between 10 and 9 kyr BP for both grounding line cases—a result very similar to those in *Uehara et al*. [2006]. For the FL scenario large drops in amplitude occur throughout the Atlantic and Indian Oceans, as well as in the Weddell and Ross Sea where amplitudes decrease locally with over 1 m. These drops coincide with the partial opening of the Nares Strait and changes in water depth of over 50 m in both the Weddell and Ross Sea due to the melting of the ice occupying these embayments (as given by changes in ICE-5G ice thicknesses). For the GR case we assume that the ice sheets in the Weddell and Ross Sea unground between 10 and 9 kyr BP. Consequently, the amplitude and dissipation rates follow the FL case from that point onward. The ungrounding event may have taken place at an earlier or later stage, but the effects are very similar regardless the timing. The ungrounding of the ice sheet in the Weddell and Ross Seas leads to a large decrease of the global total dissipation. For the GR case, these drops take a very similar pattern as for the FL case in this time step, i.e., the

dissipation decreases throughout the Atlantic, Indian Ocean, and Southern Ocean, but it is strongly enhanced around Antarctica and slightly increased throughout the remaining ocean basins. These changes in dissipation are driven by large tidal amplitudes in the Weddell and Ross Seas, and pronounced drops in amplitudes in all of the large ocean basins. The largest changes in amplitude for the FL scenario take place between 9 and 8 kyr and coincide with the retreat of large parts of the Laurentide Ice Sheet [e.g., *Dyke and Prest*, 1987]. The resulting extensive flooding led to an increase of the global shelf sea area by 2%, the largest increase over the simulation period. With the flooding of the Hudson Strait and Hudson Bay, amplitudes in the Labrador and Weddell Sea drop drastically by up to 1.5 m for both cases whereas an increase in amplitudes can be seen on the Patagonian Shelf. Large tidal amplitudes also appear in the newly formed Hudson and Nares Straits in the Canadian Arctic (Figures 8g and 8h).

3.2.1.4. 8–0 kyr BP

The last 8000 years show only small variations of the M_2 tidal amplitudes, and, consequently, only minor changes in the dissipation rates. This is consistent with results presented by *Hill et al*. [2011] and *Hall et al*. [2013] who show that tides throughout the North Atlantic showed little change during this period. Therefore, this period is not discussed further.

3.2.2. K_1 Constituent

The K_1 amplitudes and dissipation stand in contrast to the response of the M_2 tide. The K_1 amplitudes at the LGM very much resemble the present-day tidal dynamics [see *Griffiths and Peltier*, 2009]. Changes in K_1 are on a local scale as opposed the large global shifts occurring for the M_2 tide. The most prominent shifts can be seen in the Pacific where the diurnal tidal constituent is dominant at present. Consequently, we see changes in the Sea of Okhosk (SoO), the South China Sea (SCS) and the Banda Sea (BS)—the changes in these regions have also been reported by *Uehara* [2005] and *Griffiths and Peltier* [2009]. The amplitudes in the SCS and BS reach up to 1 m, and in the SoO amplitudes range up to 3 m—a pattern in contrast with PD conditions [*Zu et al*., 2008; *Green and David*, 2013]. As opposed to M_2, there are no major global differences between the different ice sheet grounding line scenarios for the LGM. The alterations in tidal dynamics are purely regional in the proximity of the respective grounding lines and the differences in global tidal amplitudes are less than 5 cm. The SCS, SoO, and BS in the Pacific are also the locations in which the largest changes occur from the LGM to the Holocene. Again, in contrast to the semidiurnal tide, these shifts take place regionally, with no large changes in the global diurnal tidal dynamics during the past 21 kyr:

3.2.2.1. 21–16 kyr BP

During this period the results from both grounding line scenarios largely resemble those during the LGM. Amplitudes in the SoO, SCS, and BS remain high, and dissipation in the North and South Pacific stays at a constant level, not reacting to the initial small increase shelf area.

3.2.2.2. 16–11 kyr BP

During this time period the largest regional shifts can be seen as shelf areas flood, thus altering local tidal dynamics. Again, the changes are confined to those basins in which the K_1 tidal constituent is dominant at present. Between 16 and 14.5 kyr BP, a gradual decrease in dissipation can be seen in the North Pacific whereas for the South Pacific the dissipation rate increases slightly with the flooding of the shelf areas in the SCS and BS (Figure 6). The decrease in the North Pacific is linked to a drop in amplitudes in the SoO and a confinement of large amplitudes to the Shelikhov Gulf as sea level continues to increase. Between 14.5 and 14.0 kyr BP a stronger drop in amplitudes in the SoO, SCS, and BS can be seen corresponding to the largest increase in sea level (20 m in 500 years) during which the Gulf of Thailand and parts of the Australian shelf flood, and a strong decrease in dissipation takes place for the North Pacific (Figures 6, 9a, and 9b). The flooding of shelf areas results in a slight increase in dissipation in the South Pacific for both scenarios. The slight drop in dissipation in the South Pacific between 13 and 12 kyr BP coincides with further flooding of the shelf areas between Japan, China, and Northern Australia. As the sea level continues to rise both scenarios gradually move toward the present-day pattern (Figures 9c and 9d) [see *Green and David*, 2013]. Between 12 and 11 kyr BP for the FL scenario the ungrounding of the ice in the Weddell and Ross Sea results in an increase in dissipation in the Southern Ocean region, and considerable amplitudes of over 1 m can now be seen in the Weddell Sea.

3.2.2.3. 11–0 kyr BP

No major changes in dissipation or amplitudes occur over this period. The small changes that can be seen again occur locally as the ice sheets gradually further unground and shallow seas are formed. Between 11

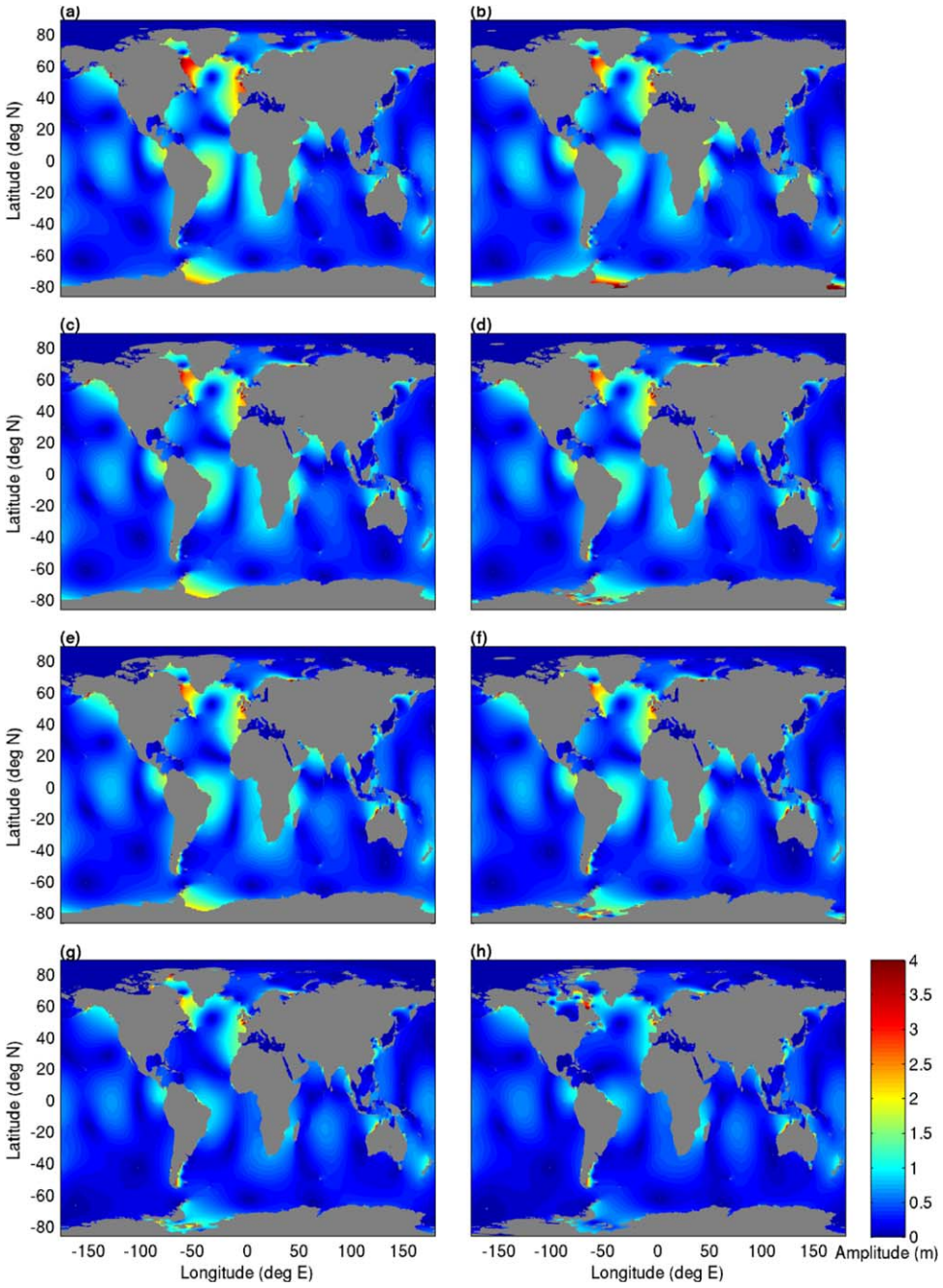

Figure 8. M_2 amplitudes at 14 kyr BP for (a) GR and (b) FL, at 11 kyr BP for (c) GR and (d) FL, at 10 kyr BP for (e) GR and (f) FL, and (g) 9 kyr BP and (h) 8 kyr BP for FL.

and 9 kyr BP, a small increase of the dissipation rates for both scenarios can be seen, which is linked to the ungrounding of the Antarctic ice sheets occupying the Weddell and Ross Sea. This is more pronounced for the GR scenario due to the larger drop in ice volume in these embayments. A small decrease in Weddell Sea amplitudes can be seen between 10 and 8 kyr BP. In contrast to the semidiurnal constituent the diurnal tides seem to have been unaffected by the large increase in sea level between 9 and 8 kyr BP (Figures 9g and 9h).

3.3. Wider Implications

The grounding line locations in the Weddell and Ross Sea appear to have a significant impact on the M_2 tidal dynamics both regionally and globally (see *Rosier et al*. [2014] for possible future effects). The situation

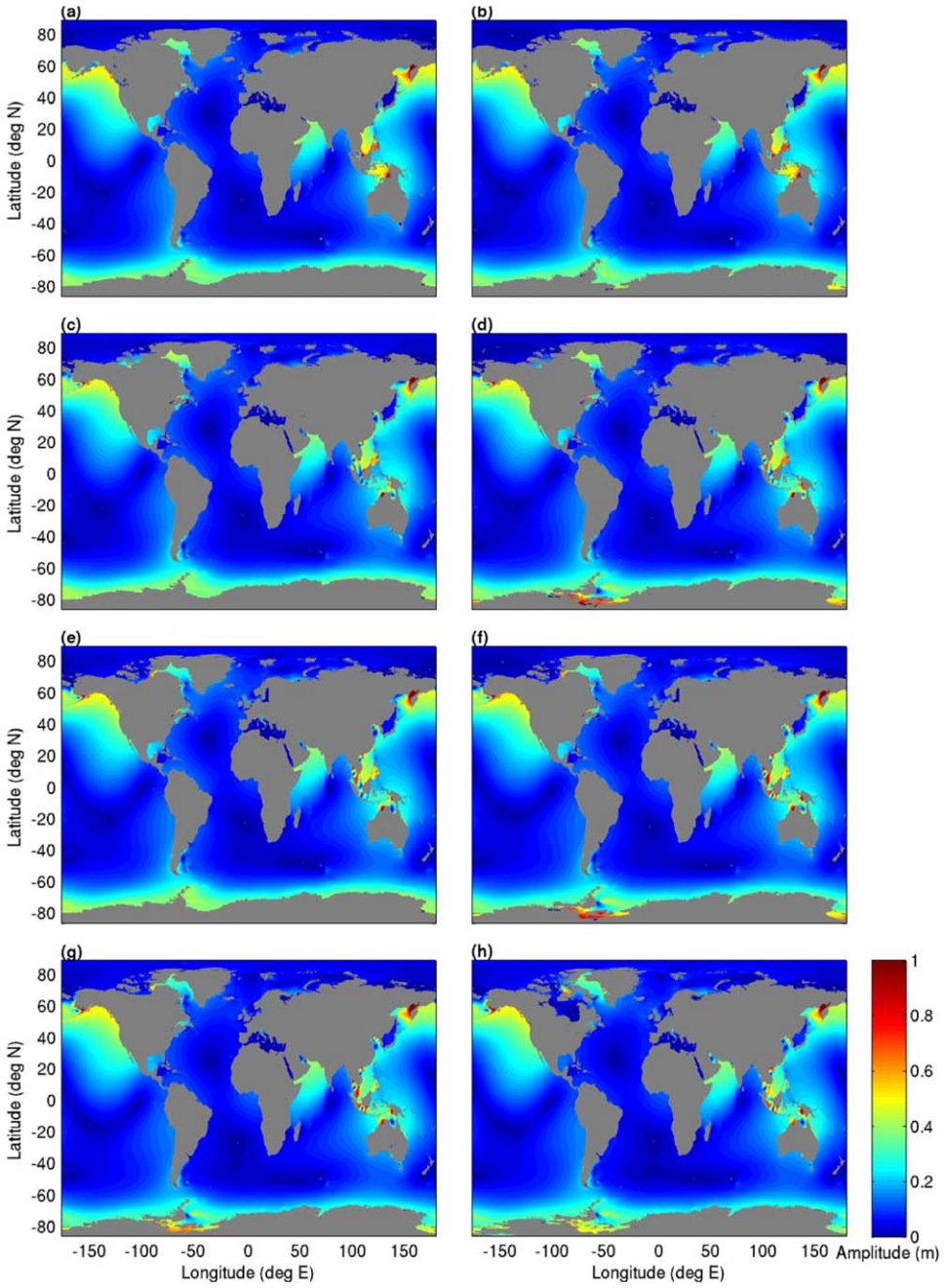

Figure 9. Same as Figure 8 but for K_1 amplitudes.

with grounded ice during the LGM gives a 1.5 times higher dissipation rate than the floating ice scenario, and was arguably the most likely configuration for the LGM. The enhanced LGM dissipation rates in the North Atlantic are thus not only due to regional resonance but also caused by feedback effects from Antarctica. This also holds for the PD simulation: if the ice shelves ground at the PD ice front, tidal dissipation rates are enhanced by a factor of 1.4 in the Northern Hemisphere, but the impact is slightly suppressed compared to the glaciation. It must be noted that this latter case is the actual bathymetry in the first version of GEBCO and highlights the importance of using accurate bathymetric databases in tidal models.

Why do K_1 and M_2 differ so strongly in their evolution from the LGM to present? In contrast to K_1, M_2 tides appear to be controlled by sea level—today a large proportion of the tidal energy dissipates in shelf seas

which were not present during the LGM. During the LGM, the North Atlantic region, the Coral Sea, the Gulf of Aden, the area north of the Mozambique Channel, and the Gulf of Panama are closer to resonance because the removal of the shelf seas acts to decrease the effective damping of the tide [*Egbert et al*., 2004; *Green*, 2010]. For the North Atlantic, continuing to lower sea level (experiments not shown here) does not increase dissipation further, suggesting that the North Atlantic is as close to resonance as it can be at the LGM. However, resonance may not be the entire story: Antarctic grounding line location appears to play a significant role in controlling global amplitudes and dissipation rates, and thus, global semidiurnal tidal dynamics. In contrast, for K_1, the areas in which large amounts of dissipation occur today—the SoO and SCS—were present during the LGM and none of the large ocean basins are close to resonance at present and during the LGM [*Platzman et al*., 1981]. This therefore leads to little change between the LGM and the present, and the responses seen are mechanistically not the same as for the M_2 constituent.

4. Discussion

With this work we present a detailed picture of the evolution of tides from the LGM to the present. Large alterations can be seen for the M_2 tidal constituent over this time period as previously suggested by a number of studies [*Egbert et al*., 2004; *Arbic et al*., 2004; *Uehara et al*., 2006; *Griffiths and Peltier*, 2009; *Green*, 2010], whereas for K_1 only small changes in the global tidal dynamics occur consistent with *Egbert et al*. [2004], *Uehara* [2005], and *Griffiths and Peltier* [2009].

In contrast to *Egbert et al*. [2004], who present time slices every 5000 years between LGM and present for M_2, we provide a much more detailed picture in 500–1000 year time intervals and we run at a much higher spatial resolution than *Uehara et al*. [2006] who present 1000 year time slices for the same period. Our simulations differ somewhat from those by *Egbert et al*. [2004] and *Uehara et al*. [2006] in that their results suggest little change in global total dissipation between 15 and 10 kyr BP. In contrast, we find that, depending on the grounding line scenario, nearly half the decrease in dissipation occurs during the transition from the LGM to the Holocene due to the large bathymetric changes resulting from the deglaciation. Furthermore, the results by *Egbert et al*. [2004] provide no indication of the exact timing of the decrease in dissipation takes place between 10 and 5 kyr BP, whereas our simulations indicate that the largest changes in dissipation take place when the ice sheets occupying the Weddell and Ross Sea unground which coincides both in timing and magnitude with the largest decreases in dissipation that *Uehara et al*. [2006] find. The largest shifts in global amplitudes take place between 9 and 8 kyr BP, when large parts of the Laurentide ice sheet disintegrated and the Hudson Bay and Straits flooded, and a large increase in sea level occurred [e.g., *Clarke et al*., 2003]. *Hill et al*. [2011] also report large changes in tidal amplitudes along the east coast of middle and Central America for this time period. Thereafter, only small changes in dissipation take place. These results highlight that the large changes in semidiurnal tides from the LGM to present did not occur linearly but are intricately tied to the ice dynamics of the major ice sheets, and their link to global sea levels.

In contrast to *Griffiths and Peltier* [2008, 2009] we do not find "megatides" in the Arctic basin during the LGM in our normal setup. Arctic tides in our simulations are enhanced by up to a factor of 5 along the north coast of Greenland and in the Canadian Basin to values only slightly smaller than reported by *Thomas and Sündermann* [1999] who find amplitudes of up to 70 cm. Increasing the TPXO7.2 elevation boundary conditions at 89°N by a factor 8 to match the amplitudes found at the same latitude by *Griffiths and Peltier* [2008, 2009], but not altering the grounding line location of the ice sheet covering the Queen Elisabeth Islands, enables us to reproduce the several metre amplitudes they find along the Arctic coastline. As *Griffiths and Peltier* [2008, 2009] use a truly global model we conclude that the Arctic megatides reported by *Griffiths and Peltier* [2008, 2009] are a likely feature. *Egbert et al*. [2004] carried out experiments with the same model we use and remark that neither changing the boundary conditions in the Arctic, placing a "vertical wall" in the center of the Arctic nor running the model in a truly global setup with the North Pole shifted into Greenland alters the global tides outside the Arctic basin which is supported by our boundary condition experiments.

Griffiths and Peltier [2008, 2009] use the ICE-5G v 1.3 paleotopography reconstruction (based on the 2min ETOPO2 present-day bathymetry) interpolated to a grid spacing that ranges from 50 km at the equator to 5 km at the poles, whereas we run with a bathymetry with a horizontal resolution of 12 km by 13.5 km at the equator to 2 km by 13.5 km horizontal resolution in the center of the Arctic Basin and superimpose the

change in topography between present day and the past time slice onto a present-day bathymetry at 1/8° resolution to retain present-day topographical features.

Our results are consistent with the damped harmonic oscillator hypothesis presented by *Egbert et al*. [2004], and further explored by *Green* [2010]. The removal of shelf seas during the LGM due to the 120 m sea-level drop reduces the damping and pushes the ocean closer to resonance, which is an effect that is especially prominent in the North Atlantic. It can be seen that notable reductions in deep dissipation occur synchronously with shelf seas flooding (e.g., at around 14 kyr BP when parts of both the Patagonian and the European Shelf flood, or between 9 and 8 kyr BP when Hudson Bay and Strait flood), meaning that the Atlantic is moved away from resonance. This agrees with work by *Arbic et al*. [2009] who show that blocking each of these three shelves in a present-day bathymetry acts to increase North Atlantic and especially Labrador Sea tides. We also show that altering the grounding line of the ice sheets in Antarctica not only has an effect on the regional tides [*Griffiths and Peltier*, 2009], but that the grounding line location also has a significant effect on the global tides, and that a change in the former can lead to notable changes in global dissipation. Our simulations therefore highlight the importance of improving the reconstructions for ice sheet extent and dynamics during the LGM and deglaciation. This is especially important as it has been hypothesized that the large tides in the Labrador Sea may have influenced the breakup of the Laurentide ice sheet during the deglaciation, and may have been one of the mechanisms of rapid ice sheet discharge of the Heinrich events during the last glacial [e.g., *Arbic et al*., 2004, 2008; *Griffiths and Peltier*, 2008, 2009]. Similarly, we suggest that the large tides found in the Weddell Sea during the LGM, for the scenarios with floating ice, could have aided in breaking up and retreating the ice from the continental shelf as also put forward by *Griffiths and Peltier* [2009] who hypothesize that the Antarctic Ice Sheet may have experienced similar instability events as the Northern Hemisphere Ice Sheets. Recent work from cores around Antarctica [*Weber et al*., 2011] indicates that the retreat of the Antarctic Ice Shelf from the shelf may have begun as early as 19.3 kyr BP in the south-eastern Weddell Sea, in an area which corresponds to the locations in which our simulations suggest large tidal amplitudes during this period.

With this work we have extended the knowledge about the K_1 tidal dynamics between the LGM and the present, the only time slices that had been explored previously [e.g., *Griffiths and Peltier*, 2008, 2009; *Green*, 2010]. In contrast to the semidiurnal tides the K_1 constituent experiences much less change between the LGM and present and between the individual time steps. Changes do not take place on a global scale but are confined to the regions in which K_1 tides are important at present, i.e., the North Pacific and especially the SoO, the SCS, and the seas around Indonesia and were also reported by *Uehara* [2005] and *Griffiths and Peltier* [2009]. Therefore, none of the dramatic shifts in dissipation that can be seen for M_2 appear for K_1. Nevertheless, considerable alterations in the tidal dynamics in these small basins can be seen. Some of these changes can be explained by shelf-blocking experiments [*Skiba et al*., 2013]. For example, blocking of the Sahul shelf enhances the tidal amplitudes in the SCS and the BS. Between 14 and 12 kyr BP when the Sahul shelf begins to flood it can be seen in our simulations that amplitudes in the Banda Sea strongly decrease. A very similar effect which is also explored by *Skiba et al*. [2013] is evident between 15 and 14 kyr BP when the Gulf of Tonkin begins to flood, and amplitudes in the South China Sea strongly decrease.

It has recently been suggested that the present tidal conversion parameterization may not be the best for this type of tidal model and that the one presented by *Nycander* [2005] gives the highest accuracy of the tidal simulation [*Green and Nycander*, 2013]. There are, however, two issues with *Nycander*'s [2005] scheme. First, it requires a 3-D stratification field for the entire ocean. For the present this is straightforward, and one could possibly use results from a paleomodel for the LGM field, but we still lack relevant data for the other time slices between the LGM and PD. Furthermore, *Egbert et al*. [2004] showed that increasing the global conversion coefficient with factors between 0.5 and 4 had relatively small effects on the global dissipation rates during the LGM. This is to some extent supported by *Green and Huber* [2013], who show that during the early Eocene (50 Ma) the abyssal M_2 dissipation rates were twice as large as at present even though the vertical stratification was 3–4 times stronger than today. One could of course argue that we could use Nycander's scheme but with a slightly modified PD stratification all the way through, but the second problem with using Nycander's parameterization is that of resolution. The conversion coefficient C_w in equation (1) must be computed at at least 1/30° resolution for Nycander's parameterization to be accurate, which is far too detailed for the paleo-slices, and consequently we have to rely on other parameterizations at the moment. To obtain a likely range of the LGM dissipation rates and highlight the insensitivity, we repeated

the sensitivity analysis by *Egbert et al*. [2004] and multiplied the conversion coefficient by a factor 0.5 or 2. There is an associated change in the abyssal dissipation—in both our results and those by *Egbert et al*. [2004]—but only with some 10–15% either way (see the diamonds and squares in Figures 7b and 7c) and the changes in global average amplitudes lie in the order of 20% either way. This is because of the coupling in the model: when the IT drag is reduced, the velocity field may increase which leads to an increased dissipation and decreased amplitudes (and vice versa for an increased drag). These results show that the abyssal tidal dissipation rates are relatively insensitive to changes in hydrography, and the modified IT-drag runs presented give a quite probable range of paleo-dissipation rates and amplitudes in the ocean.

Predictions of sea-level rise over the present century range significantly, but most lie between 0.75 and 1.9 m for the period 1990–2100 [*Bindoff et al*., 2007; *Pfeffer et al*., 2008; *Vermeer and Rahmstorf*, 2009], although there are large uncertainties. A 2 m future sea-level rise would flood some 1.5% of the present-day dry land—a number roughly corresponding to the peak in shelf area 4 kyr BP. There is therefore a potential for even moderate future sea-level rise to have far-reaching effects, not only on regional tides [e.g., *Ward et al*., 2012; *Pelling et al*., 2013] but also on the global tides. These regional studies imply that the tides are sensitive to the way future sea-level rise is implemented, and they stress the need for high-resolution simulations of global tides.

Acknowledgments

J.A.M.G. acknowledges funding from the Natural Environmental Research Council through grant NE/F014821/1 and from the Climate Change Consortium for Wales. S.B.W. received a PhD studentship from Fujitsu through HPC Wales, who also provided computer facilities. Discussions with John Simpson, James Scourse, and Adam Wainwright improved the manuscript and Ade Fewings at HPC Wales provided invaluable technical support.

References

Amante, C., and B. W. Eakins (2009), ETOPO1 1 Arc-Minute Global Relief Model: Procedures, data sources and analysis, *NOAA Tech. Memo. NESDIS NGDC 24*, 19 pp., National Geophysical Data Center, NOAA, doi:10.7289/V5C8276M.

Anderson, J. B., S. S. Shipp, A. L. Lowe, J. S. Wellner, and A. B. Mosola (2002), The Antarctic ice sheet during the Last Glacial Maximum and its subsequent retreat history: A review, *Quat. Sci. Rev.*, *21*, 49–70, doi:10.1016/S0277-3791(01)00083-X.

Arbic, B. K., D. R. Macayeal, J. X. Mitrovica, and G. A. Milne (2004), Paleoclimate: Ocean tides and Heinrich events, *Nature*, *432*, 460.

Arbic, B. K., P. St-Laurent, G. Sutherland, and C. Garrett (2007), On the resonance and influence of the tides in Ungawa Bay and Hudson Strait, *Geophys. Res. Lett.*, *34*, L17606, doi:10.1029/2007GL030845.

Arbic, B. K., J. X. Mitrovica, D. R. MacAyeal, and G. A. Milne (2008), On the factors behind large Labrador Sea tides during the last glacial cycle and the potential implications for Heinrich events, *Paleoceanography*, *23*, PA3211, doi:10.1029/2007PA001573.

Arbic, B. K., R. H. Karsten, and C. Garrett (2009), On tidal resonance in the global ocean and the back-effect of coastal tides upon open-ocean tides, *Atmos. Ocean*, *47*, 239–266, doi:10.3137/OC311.2009.

Bindoff, N. L., et al. (2007), Observations: Oceanic climate change and sea level, in *Climate Change 2007: The Physical Science Basis. Contribution of Working Group I to the Fourth Assessment Report of the Intergovernmental Panel on Climate Change*, edited by S. Solomon et al., pp. 387–432, Cambridge Univ. Press, Cambridge, U. K.

Broecker, W. S., and G. H. Denton (1990), What drives glacial cycles, *Sci. Am.*, *262*(1), 48–56.

Clarke, G., D. Leverington, J. Teller, and A. Dyke (2003), Paleoclimate. Superlakes, megafloods, and abrupt climate change, *Science*, *301*(5635), 922–923, doi:10.1126/science.1085921.

Domack, E. W., E. A. Jacobson, S. Shipp, and J. B. Anderson (1999), Late Pleistocene - Holocene retreat of the West Antarctic Ice-Sheet system in the Ross Sea: Part 2—Sedimentologic and stratigraphic signature, *Geological Society of America Bulletin*, *111*(10), 1517–1536, doi:10.1130/0016–7606(1999)111.1517.

Dyke, A. S., and V. K. Prest (1987), Late Wisconsinan and Holocene history of the Laurentide ice sheet, *Geogr. Phys. Quaternaire*, *41.2*, 237–263.

Egbert, G. D., and S. Y. Erofeeva (2002), Efficient inverse modeling of barotropic ocean tides, *J. Atmos. Oceanic Technol.*, *19*, 183–204.

Egbert, G. D., and R. D. Ray (2001), Estimates of M2 tidal energy dissipation from Topex/Poseidon altimeter data, *J. Geophys. Res.*, *106*, 22,475–22,502.

Egbert, G. D., B. G. Bills, and R. D. Ray (2004), Numerical modeling of the global semidiurnal tide in the present day and in the Last Glacial Maximum, *J. Geophys. Res.*, *109*, C03003, doi:10.1029/2003JC001973.

Green, J. A. M. (2010), Ocean tides and resonance, *Ocean Dyn.*, *60*(5), 1243–1253, doi:10.1007/s10236-010-0331-1.

Green, J. A. M., and G. R. Bigg (2011), Impacts on the global ocean circulation from vertical mixing and a collapsing Ice Sheet, *J. Mar. Res.*, *69*, 1–24.

Green, J. A. M., and M. Huber (2013), Tidal dissipation in the early Eocene and implications for ocean mixing, *Geophys. Res. Lett.*, *40*, 2707–2713, doi:10.1002/grl.50510.

Green, J. A. M., and J. Nycander (2013), A comparison of tidal conversion parameterizations for tidal models, *J. Phys. Oceanogr.*, *43*(1), 104–119, doi:10.1175/JPO-D-12–023.1.

Green, J. A. M., C. L. Green, G. R. Bigg, T. P. Rippeth, J. D. Scourse, and K. Uehara (2009), Tidal mixing and the meridional overturning circulation from the Last Glacial Maximum, *Geophys. Res. Lett.*, *36*, L15603, doi:10.1029/2009GL039309.

Green, J. M., and T. W. David (2013), Non-assimilated tidal modeling of the South China Sea, *Deep Sea Res., Part I*, *78*, 42–48, doi:10.1016/j.dsr.2013.04.006.

Griffiths, S. D., and W. R. Peltier (2008), Megatides in the Arctic Ocean under glacial conditions, *Geophys. Res. Lett.*, *35*, L08605, doi:10.1029/2008GL033263.

Griffiths, S. D., and W. R. Peltier (2009), Modeling of polar ocean tides at the Last Glacial Maximum: Amplification, sensitivity, and climatological implications, *J. Clim.*, *22*, 2905–2924, doi:10.1175/2008JCLI2540.1.

Hall, B. L., and G. H. Denton (2000), Extent and chronology of the Ross sea ice sheet and the Wilson Piedmont Glacier along the Scott Coast at and since the Last Glacial Maximum, *Geogr. Ann., Ser. A*, *82A*, 337–363, doi:10.1111/1468-0459.00128.

Hall, G. F., D. F. Hill, B. P. Horton, S. E. Engelhart, and W. R. Peltier (2013), High-resolution study of tides in Delaware Bay: Past conditions and future scenarios, *Geophys. Res. Lett.*, *40*, 338–342, doi:10.1029/2012GL054675.

Hein, A. S., C. J. Fogwill, D. E. Sugden, and S. Xu (2011), Glacial/interglacial ice-stream stability in the Weddell Sea embayment, Antarctica, *Earth Planet. Sci. Lett.*, *307*(1–2), 211–221, doi:10.1016/j.epsl.2011.04.037.
Hill, D. F., S. D. Griffiths, W. R. Peltier, B. P. Horton, and T. E. Törnqvist (2011), High-resolution numerical modelling of tides in the western Atlantic, Gulf of Mexico, and Caribbean Sea during the Holocene, *J. Geophys. Res.*, *116*, C10014, doi:10.1029/2010JC006896.
Hillenbrand, C.-D., M. Melles, G. Kuhn, and R. D. Larter (2012), Marine geological constraints for the grounding-line position of the Antarctic Ice Sheet on the southern Weddell Sea shelf at the Last Glacial Maximum, *Quat. Sci. Rev.*, *32*, 25–47, doi:10.1016/j.quascirev.2011.11.017.
Huang, R. X. (1999), Mixing and energetics of the oceanic thermohaline circulation, *J. Phys. Oceanogr.*, *29*, 727–746.
Jakobsson, M., R. Macnab, L. Mayer, R. Anderson, M. Edwards, J. Hatzky, H. W. Schenke, and P. Johnson (2008), An improved bathymetric portrayal of the Arctic Ocean: Implications for ocean modeling and geological, geophysical and oceanographic analyses, *Geophys. Res. Lett.*, *35*, L07602, doi:10.1029/2008GL033520.
Johnson, G. C., S. G. Purkey, and J. M. Toole (2008), Reduced Antarctic meridional overturning circulation reaches the North Atlantic Ocean, *Geophys. Res. Lett.*, *35*, L22601, doi:10.1029/2008GL035619.
Larter, R. D., A. G. Graham, C.-D. Hillenbrand, J. A. Smith, and J. A. Gales (2012), Late Quaternary grounded ice extent in the Filchner Trough, Weddell Sea, Antarctica: New marine geophysical evidence, *Quat. Sci. Rev.*, *53*, 111–122, doi:10.1016/j.quascirev.2012.08.006.
Lenderink, G., and R. J. Haarsma (1994), Variability and multiple equilibria of the thermohaline circulation, associated with deep water formation, *J. Phys. Oceanogr.*, *24*, 1480–1493.
Livingstone, S. J., C. Ó. Cofaigh, C. R. Stokes, C.-D. Hillenbrand, A. Vieli, and S. S. Jamieson (2012), Antarctic palaeo-ice streams, *Earth Sci. Rev.*, *111*(1–2), 90–128, doi:10.1016/j.earscirev.2011.10.003.
McKay, R., G. Dunbar, T. Naish, P. Barrett, L. Carter, and M. Harper (2008), Retreat history of the Ross Ice Sheet (Shelf) since the Last Glacial Maximum from deep-basin sediment cores around Ross Island, *Palaeogeogr. Palaeoclimatol. Palaeoecol.*, *260*(1–2), 245–261, doi:10.1016/j.palaeo.2007.08.015.
Mosola, A. B., and J. B. Anderson (2006), Expansion and rapid retreat of the West Antarctic Ice Sheet in eastern Ross Sea: Possible consequence of over-extended ice streams?, *Quat. Sci. Rev.*, *25*(17–18), 2177–2196, doi:10.1016/j.quascirev.2005.12.013.
Müller, M. (2008), Synthesis of forced oscillations, Part I: Tidal dynamics and the influence of the loading and self-attraction effect, *Ocean Modell.*, *20*, 207–222.
Nycander, J. (2005), Generation of internal waves in the deep ocean by tides, *J. Geophys. Res.*, *110*, C10028, doi:10.1029/2004JC002487.
Pelling, H. E., and J. A. M. Green (2013), Sea level rise and tidal power plants in the Gulf of Maine, *J. Geophys. Res. Oceans*, *118*, 2863–2873, doi:10.1002/jgrc.20221.
Pelling, H. E., J. A. M. Green, and S. L. Ward (2013), Modelling tides and sea-level rise: To flood or not to flood, *Ocean Modell.*, *63*, 21–29, doi:10.1016/j.ocemod.2012.12.004.
Peltier, W. (2004), Global glacial isostasy and the surface if the ice-age earth: The ICE-5G (VM2) model and Grace, *Annu. Rev. Earth Planet. Sci.*, *32*, 111–149.
Pfeffer, W. T., J. T. Harper, and S. O'Neel (2008), Kinematic constraints on glacier contributions to 21st-century sea-level rise, *Science*, *321*, 1340–1342, doi:10.1126/science.1159,099.
Platzman, G. W. (1975), Normal modes of the Atlantic and Indian Oceans, *J. Phys. Oceanogr.*, *5*, 201–221.
Platzman, G. W., G. A. Curtis, K. S. Hansen, and R. D. Slater (1981), Normal modes of the world ocean 2. Description of modes in the periods range 8 to 80 hours, *J. Phys. Oceanogr.*, *11*, 579–603.
Rahmstorf, S. (2002), Ocean circulation and climate during the past 120,000 years, *Nature*, *419*, 207–214.
Rosier, S. H. R., J. A. M. Green, J. D. Scourse, R. Winkelmann (2014), Modeling Antarctic tides in response to ice shelf thinning and retreat, *J. Geophys. Res. Oceans*, *119*, 87–97, doi:10.1002/2013JC009240.
Shipp, S., J. B. Anderson, and E. W. Domack (1999), Late Pleistocene-Holocene retreat of the west Antarctic ice-sheet system in the ross sea: Part 1—Geophysical results, *Geol. Soc. Am. Bull.*, *111*, 1486–1516, doi:10.1130/0016-7606(1999)111-1486.
Skiba, A. W., L. Zeng, B. K. Arbic, M. Müller, and W. J. Godwin (2013), On the resonance and shelf/open-ocean coupling of the global diurnal tides, *J. Phys. Oceanogr.*, *43*(7), 1301–1324, doi:10.1175/JPO-D-12-054.1.
Smith, W. H., and D. T. Sandwell (1997), Global sea floor topography from satellite altimetry and ship depth soundings, *Science*, *277*(5334), 1956–1962, doi:10.1126/science.277.5334.1956.
Stolldorf, T., H.-W. Schenke, and J. B. Anderson (2012), LGM ice sheet extent in the Weddell Sea: Evidence for diachronous behavior of Antarctic Ice Sheets, *Quat. Sci. Rev.*, *48*, 20–31, doi:10.1016/j.quascirev.2012.05.017.
Stommel, H. M. (1961), Thermohaline convection with two stable regimes, *Tellus*, *13*, 224–230.
Thomas, M., and J. Sündermann (1999), Tides and tidal torques of the world since the Last Glacial Maximum, *J. Geophys. Res.*, *104*, 3159–3183.
Uehara, K. (2005), Changes of ocean tides along Asian coasts caused by the post glacial sea-level change, in *Mega-Deltas of Asia: Geological Evolution and Human Impact*, edited by Z. Chen, Y. Saito, and S. L. Goodbred Jr., pp. 227–232, China Ocean Press, Beijing, China.
Uehara, K., J. D. Scourse, K. J. Horsburgh, K. Lambeck, and A. P. Purcell (2006), Tidal evolution of the northwest European shelf seas from the Last Glacial Maximum to the present, *J. Geophys. Res.*, *111*, C09025, doi:10.1029/2006JC003531.
Vermeer, M., and S. Rahmstorf (2009), Global sea level linked to global temperature, *Proc. Natl. Acad. Sci. U. S. A.*, *106*, 21,527–21,532.
Ward, S. L., J. A. M. Green, and H. E. Pelling (2012), Tides, sea-level rise and tidal power extraction on the European shelf, *Ocean Dyn.*, *62*, 1153–1167, doi:10.1007/s10236-012-0552-6.
Weber, M. E., W. Ricken, P. U. Clark, G. Kuhn, S. W. Hostetler, and J. X. Mitrovica (2011), Interhemispheric ice-sheet synchronicity during the Last Glacial Maximum, *Sciences*, *336*, 1265–1269, doi:10.1126/science.1209299.
Zaron, E. D., and G. D. Egbert (2006), Estimating open-ocean barotropic tidal dissipation: The Hawaiian Ridge, *J. Phys. Oceanogr.*, *36*, 1019–1035.
Zu, T., J. Gan, and S. Y. Erofeeva (2008), Numerical study of the tide and tidal dynamics in the South China Sea, *Deep Sea Res., Part I*, *55*(2), 137–154, doi:10.1016/j.dsr.2007.10.007.